CHEMISTRY
A EUROPEAN JOURNAL

DOI: 10.1002/chem.201001218

Dynamic Calcium Metal–Organic Framework Acts as a Selective Organic Solvent Sponge

Ana E. Platero-Prats,[a] Víctor A. de la Peña-O'Shea,[b] Natalia Snejko,[a] Ángeles Monge,[a] and Enrique Gutiérrez-Puebla*[a]

Abstract: Herein, we present a Ca-based metal–organic framework named AEPF-1, which is an active and selective catalyst in olefin hydrogenation reactions. AEPF-1 exhibits a phase transition upon desorption of guest molecules. This structural transformation takes place by a crystal to crystal transformation accompanied by the loss of single-crystal integrity. Powder diffraction methods and computational studies were applied to determine the structure of the guest-free phase. This work also presents data on the exceptional adsorption behavior of this material, which is shown to be capable of separating polar from nonpolar organic solvents, and is a good candidate for selective solvent adsorption under mild conditions.

Keywords: crystal engineering · crystal transformations · dynamic porous materials · host–guest systems · metal–organic frameworks

Introduction

During recent years, great attention has been paid to the design and synthesis of porous metal–organic frameworks (MOFs) due to their high versatility, and their many potential applications in areas such as gas storage and separation, sensors, heterogeneous catalysis, and drug delivery.[1–7] Within this field, one of the main challenges is the synthesis and the study of dynamic MOFs, the so-called third-generation compounds, which exhibit interesting properties on response to stimuli (heat, pressure, light, external molecules, etc.).[8,9] Some interesting porous MOFs have been reported[10,11] that can change their porosity in various ways; for example, by reversible collapse and recovery of pores, or through structural changes. This dynamic structural behavior is of great importance, because these flexible materials can exhibit high selectivity for guest inclusion, selective molecular recognition, or drug-delivery properties, among others, as mentioned above.[12,13]

A suitable guest can induce the formation of a specific framework, thereby playing an important role in the dynamic changes in the framework. Guest removal can also lead to structural changes in the host framework, which normally gives rise to phase transitions. On the other hand, the original structure can often be restored by exposing the dry material to the guest again. These structural transformations can take place as 1) single-crystal to single-crystal transformations[14,15] or 2) crystal to crystal (CC) (losing the single crystal integrity) transformations. To appreciate the structural features of these guest-induced transformations, X-ray powder diffraction (XRPD) methods and computational methods need to be applied.[16]

MOFs based on alkaline-earth metals remain a scientific challenge because of the inherent difficulties concerning the formation and crystallization of these MOFs.[17] In fact, few examples of rigid MOFs based on calcium have yet been reported.[18–20] However, flexible materials based on alkaline-earth metals could represent a comparatively cheap, nontoxic, green alternative to conventional transition-metal-based dynamic MOFs.

Recently, we have prepared a Ca-MOF named AEPF-1 (in which AEPF = alkaline-earth polymer framework), based on the organic linker 4,4′-(hexafluoroisopropylidene)-

[a] A. E. Platero-Prats, Dr. N. Snejko, Prof. Á. Monge, Prof. E. Gutiérrez-Puebla
New Architectures in Materials Chemistry
Instituto de Ciencia de Materiales de Madrid (ICMM-CSIC)
C/Sor Juana de la Cruz 3, Cantoblanco, Madrid (Spain)
Fax: (+34) 913720623
E-mail: egutierrez@icmm.csic.es

[b] Dr. V. A. de la Peña-O'Shea
Thermochemical Processes Group
Instituto Madrileño de Estudios Avanzados en Energía (IMDEA Energía), C/Tulipán s/n Móstoles
Madrid (Spain)

Supporting information for this article is available on the WWW under http://dx.doi.org/10.1002/chem.201001218.

bis(benzoic acid) (H_2hfipbb = $C_{17}H_{10}O_4F_6$), in which an sp^3 carbon atom joins the two benzoic moieties, rendering it flexible. Our preliminary catalytic tests showed that AEPF-1 is an active and selective catalyst in olefin hydrogenation and hydrosilylation reactions.[21] The catalyst is an economical and environmentally friendly alternative to conventional catalysts based on precious metals. Herein, we report a summary of the synthesis, structure, and catalytic activity of this new Ca-MOF, as well as new results based on its reversible structural CC transformation, the new structure of the AEPF-1 dry-phase (AEPF-1_{dry}) solved by XRPD and computational studies, and the application of AEPF-1 as a selective absorbent of organic solvents under mild conditions.

Results and Discussion

The three-dimensional framework of AEPF-1 was synthesized from the solvothermal reaction of [$Ca(CH_3CO_2)_2 \cdot H_2O$] and H_2hfipbb in a water/acetone mixture, which resulted in the formation of single crystals of a new MOF with formula [Ca(hfipbb)(H_2hfipbb)$_{0.5}$(H_2O)]·0.5 C_3H_6O, (in which hfipbb is the deprotonated form of H_2hfipbb) in around 70% yield. The structure has been solved by single-crystal X-ray diffraction experiments, which showed that it consists of a monocapped octahedral calcium polyhedron that forms Ca_2O_{12} edge-sharing dimeric units, which are linked by the dibenzoic carboxylate ligand along the *b* direction. These chains are joined through the whole deprotonated linker hfipbb^{2-}, forming layers with square-shaped channels along the [101] direction, and joined along the [−101] direction through the protonated linker H_2hfipbb (see Figure 3 and Table S1 and Figure S1 in the Supporting Information). This arrangement gives rise to a 3D framework. Three characteristics of this calcium-based MOF are noteworthy: 1) it has a porous structure, possessing cavities with an accessible free space of $V = 157$ Å^3 and a pore-size diameter of 6.9 Å (calculated with PLATON, taking into account the van der Waals radii);[22] 2) the results of our previous tests (Figure S14 in the Supporting Information) showed that AEPF-1 is an active catalyst: total conversion of styrene proceeds, with 100% selectivity, to the hydrogenated product ethyl benzene in 2 h, by using 1 mol% of catalyst at 373 K and 5 atm H_2;[21] 3) AEPF-1 contains acetone as guest molecules, which are held inside pores through soft interactions, and can be removed by heating (Figure S2 in the Supporting Information). Hence, the reversible uptake–release behavior of guest molecules in AEPF-1 would demonstrate the potential application of this material as an absorber, or as an organic-molecule sensor. Such studies have been reported for transition-metal-based MOFs,[16] but not for alkaline-earth-metal MOFs.

Study of AEPF-1 activation: To investigate the potential application of this material for adsorption, a detailed study of AEPF-1 activation processes was performed following the loss of guest molecules from its pores, as follows: A thermal study of AEPF-1 was carefully performed in the temperature range 20–200 °C by using thermogravimetric analysis (TGA) combined with mass spectrometry (TGA-MS) and differential scanning calorimetry (DSC). Within the temperature range explored, the weight loss was attributed to 1) physisorbed water and acetone molecules (up to 75 °C), and 2) guest molecules from pores (up to 200 °C), corresponding to two acetone molecules per unit cell (Figure S4 in the Supporting Information). Above this temperature, the material is stable up to 400 °C (see the Supporting Information). A change in the weight-loss rate was observed at around 75 °C. This weight-loss rate reflects the departure of acetone from pores. It continues up to around 105 °C (T_c), where the weight-loss rate changes again. These results are in accordance with recent studies,[18] which show a two-step departure of acetone molecules that could be associated with structural changes in the framework. Furthermore, DSC has been used as a complementary tool to explore the energetic processes involved in the acetone departure from the pores in AEPF-1 (see Figure S4 in the Supporting Information for details). A single peak centered at 105 °C (T_c) is observed. This process is composed of two simultaneous steps: 1) acetone loss from the pores; and 2) structural changes in the AEPF-1 framework.[23]

To determine the intrinsic energy involved in the guest removal process, a series of computational studies was performed by using the AEPF-1 atomic coordinates determined by single-crystal XRD. All structural models were optimized by using plane wave density functional calculations (PWDF) (see the Experimental Section). Geometry optimization of AEPF-1 converged to the same structure as determined by X-ray crystallography, which confirms the accuracy of the calculation method. These theoretical calculations allowed the guest desorption apparent energy to be estimated at 25.5 kJ mol^{-1}.[24]

Taking into account the results of the activation process of AEPF-1, along with those of our previous studies, a detailed structural study was performed to elucidate the effect on the crystal structure on the guest removal process. This entailed a series of experiments using variable-temperature optical microscopy (VTOM), variable-temperature diffuse reflectance Fourier-transform infrared spectroscopy (VT-DRIFTS), and X-ray powder thermodiffraction (XRPTD).

Variable-temperature optical microscopy: To study the variations in crystallinity accompanying the guest removal process in AEPF-1, VTOM experiments were performed (see the Experimental Section and the Supporting Information, Section S3). Thus, a single crystal of AEPF-1 was heated from room temperature to 150 °C. At around 75 °C the crystal began to decay, which corresponds to removal of guest molecules from the pores (Figure 1B), as described above. Subsequent temperature increase to 105 °C causes the total loss of single-crystal integrity, although the crystal retains its shape (Figure 1F), a phenomenon that gives rise to typical microcrystalline X-ray diffraction diagrams. These results confirm that possible structural changes related to the guest

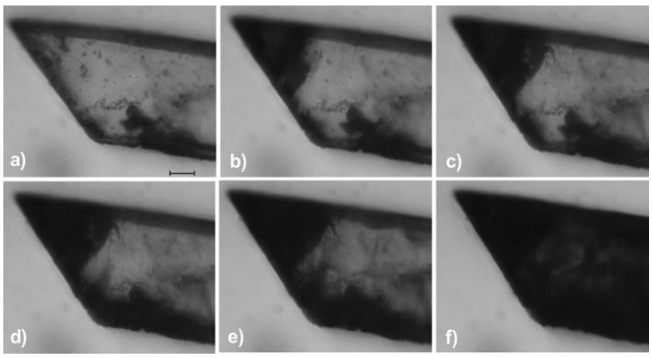

Figure 1. Optical microphotographs of a single crystal of AEPF-1 at a) room temperature, b) 75 °C, c) 82 °C, d) 90 °C, e) 97 °C, f) 105 °C. (For details, see the Supporting Information, Section S3.) Scale bar is 20 μm.

removal process cannot be followed by single-crystal diffraction studies for AEPF-1.

X-ray powder thermodiffraction: To accurately follow the structural changes accompanying the acetone removal process in AEPF-1, XRPTD experiments were performed (see the Experimental Section). These studies show that when the temperature reaches 75 °C, new peaks corresponding to an unknown crystalline phase (named AEPF-1_{dry}) appear together with those peaks associated with the AEPF-1 phase. As the temperature is further increased, the intensity of the AEPF-1 peaks decreases, whereas that of the AEPF-1_{dry} peaks increases; these two phases coexist up to 95 °C. Finally, at temperatures above 100 °C only the peaks of the AEPF-1_{dry} phase could be observed. These experiments confirm that the host material exhibits a structural transformation due to the loss of guest molecules (Figure 2A and 2B), which gives rise to AEPF-1_{dry} with formula $[CaC_{25.5}F_9O_6H_{15}]_\infty$, as determined by elemental analysis (see the Experimental Section).

Variable-temperature diffuse reflectance Fourier-transform infrared spectroscopy: VT-DRIFTS studies were carried out at temperatures up to 130 °C (see the Experimental Section). At room temperature, typical υ_{CO} vibrations corresponding to the carbonyl groups of free acetone (present in the pores of the framework) are observed at 1715 cm^{-1}. As the temperature is raised, a slight blueshift of the acetone band is observed (1720 cm^{-1}), while its intensity decreases (Figure 2C). Finally, above 120 °C, no band corresponding to

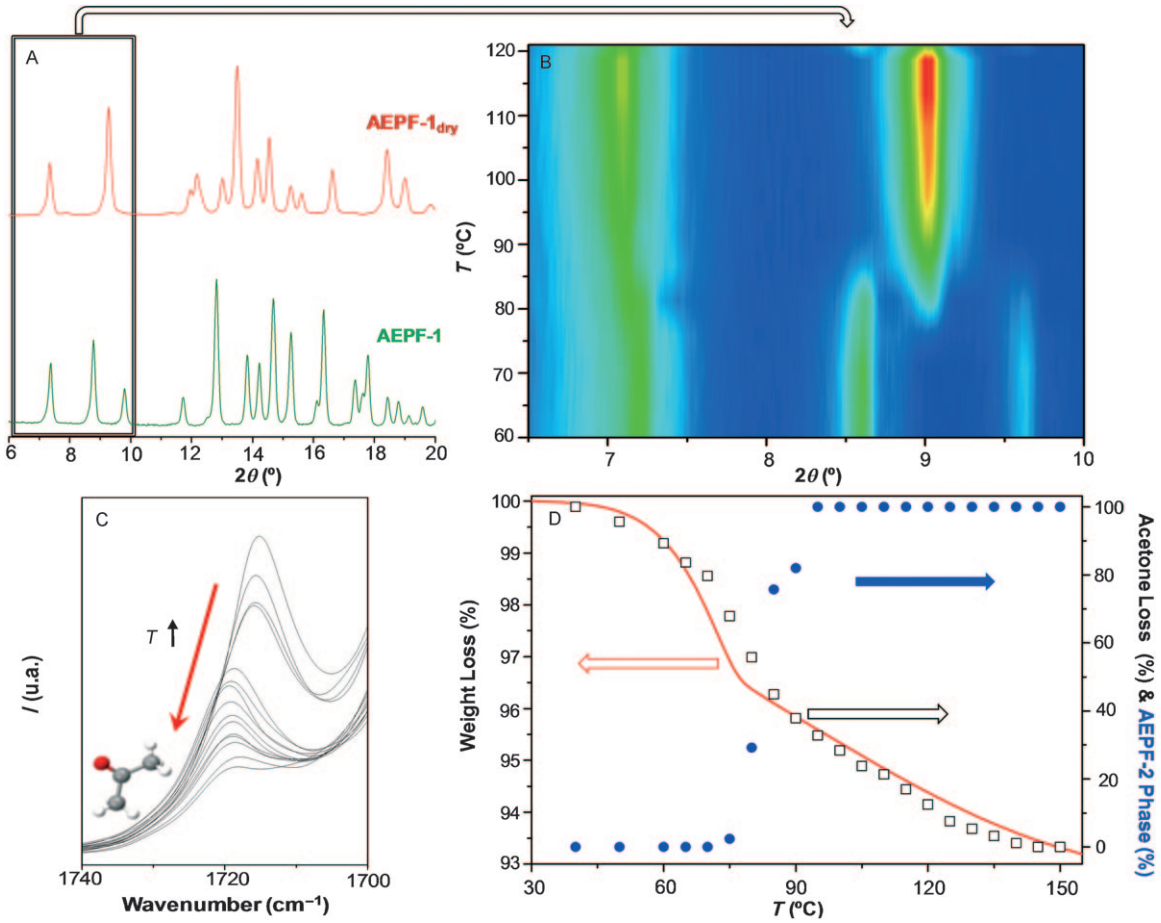

Figure 2. A) XRPD patterns of AEPF-1 (red) and AEPF-1_{dry} (green). B) XRPTD experiments that show the transformation of AEPF-1 to AEPF-1_{dry} increases with the temperature. C) Change in the IR spectrum of AEPF-1 versus temperature, in the region of υ_{CO} for free acetone, due to the acetone loss. D) Plot of the ratio of AEPF-1_{dry} (blue), acetone loss (black), and weight loss (red) versus temperature.

acetone is observed. This variation was used to calculate the loss of acetone in AEPF-1 (Figure 2C). At room temperature, the bands corresponding to the υ_{CO} vibrations of the carboxylate groups of AEPF-1 were observed at 1687, 1609 (1595) ($\eta^2\mu_3$ mode), and 1562 (1547) cm^{-1} ($\eta^2\mu_2$ mode), which is consistent with the coordination modes of the carboxylate groups determined by single-crystal XRD. Upon increasing the temperature, the bands in this range are observed at 1682, 1662, 1611, and 1566 cm^{-1}. These results confirm that structural changes take place during guest removal (see the Supporting Information, Figure S5).

To summarize the variable-temperature studies results, a plot of the ratio of AEPF-1_{dry} (calculated from XRPD data), the acetone loss (calculated from IR data), and the weight loss (calculated from TGA data) versus temperature are shown in Figure 2. A clear relationship between the weight loss due to acetone removal and the phase transition from AEPF-1 to AEPF-1_{dry} is observed.

Structure determination of AEPF-1_{dry}: Because guest removal caused single-crystal decay, the structure of AEPF-1_{dry} was determined by XRPD and computational methods. The XRPD pattern of AEPF-1_{dry} shows clear peak overlap and a lack of peaks at high Bragg angles. Nevertheless, the pattern was indexed by using the DICVOL04 program[25,26] in an orthorhombic unit cell with $a=31.55$, $b=24.64$, and $c=7.37$ Å, and $V=5731.7$ Å^3 (figures of merit $M_{20}=10$, $F_{20}=24$). However, after carefully studying the systematic absences, the monoclinic system was chosen with β angle close to 90° and the space group was determined to be $P2/c$ ($Z=4$). A matrix transformation was then applied to obtain the correct monoclinic unit cell with $a=24.64$, $b=7.37$, and $c=31.55$ Å, and $\beta=90°$.

First, a Pawley profile fitting procedure,[27] which employed the Materials Studio software,[28] was used to refine the cell and peak-profile parameters, as well as those of the background, peak asymmetry, and zero shift. Then, a crystal-structure model could be obtained by using the direct-space global optimization algorithms implemented in the computer program FOX.[29,30] Since the unit cell volume of AEPF-1_{dry} ($V_{AEPF\text{-}1dry}$) is, approximately, twice that of the unit cell volume of AEPF-1 ($V_{AEPF\text{-}1}$), a valid chemical model consisting of two AEPF-1 asymmetric units was used. The best of the AEPF-1_{dry} models generated by FOX was then optimized by Rietveld refinement[31] (considering molecules as rigid bodies) with energy optimization (Pareto optimization), using the Reflex module of the Materials Studio software. This method tries to balance matching the simulated pattern with the experimental diffraction data and then to minimize the potential energy of the structure.

Then, subsequent Rietveld refinements were performed by using only gradually relaxed constraints (some torsion angles were relaxed) to keep the model chemically sensible. Finally, hydrogen atoms were geometrically situated to complete the model. Refinement of this model converged with the R values $R_{wp}=0.186$ and $R_p=0.263$. Finally, to determine a chemically consistent structure of the dry phase PWDF calculations were carried out (see the Experimental Section). The initial coordinates of AEPF-1_{dry} were taken from the final refined structural model obtained by XRPD.

A structure minimization calculation was performed in the space group $P1$ by keeping the cell parameters fixed. The newly obtained structural model was then optimized, as mentioned above, by using Rietveld methodology. Refinement of this model converged with R values $R_{wp}=0.115$ and $R_p=0.156$. The final refined cell parameters are $a=24.644$, $b=7.382$, and $c=31.578$ Å, with $\beta=90.17°$. This study has given rise to a structural model of the dry phase that is chemically consistent and consistent with the crystal structure, despite the complexity of the structure. Details of the unit cell and the refinement of AEPF-1_{dry} are given in Table S2 (see also the Experimental Section).

The structural model of AEPF-1_{dry} contains two independent calcium atoms: one is hepta-coordinated, and forms a monocapped octahedron, as it does in AEPF-1; however, the other calcium center is hexa-coordinated, forming a monocapped trigonal bipyramidal distorted polyhedron, the vertices of which are occupied by four oxygen atoms; two from completely deprotonated hfipbb^{2-} ligands, one from a protonated H_2hfipbb ligand, and one from a water molecule. It is remarkable that the coordination modes of carboxylate groups from deprotonated hfipbb^{2-} ligands in AEPF-1_{dry} ($\eta^2\mu_3$ (chelate bridge), $\eta^2\mu_2$ (bridge), and $\eta^1\mu_1$ (monodentate)) are different from those in AEPF-1 ($\eta^2\mu_3$ (chelate bridge) and $\eta^2\mu_2$ (bridge)). Moreover, a hydrogen bond between a coordinated water molecule and the monodentate carboxylate group is found (with $d_{O10\text{–}O2}=2.688$ Å) for AEPF-1_{dry}. It was also found that the loss of acetone molecules involves changes in the torsion angles of the organic ligand: along the c direction, all ligands have the same orientation (for AEPF-1 the torsion angle is C_{21}-C_{22}-C_{25}-C_{22}= 44.23°; for AEPF-1_{dry}, it is C_{46}-C_{45}-C_{42}-C_{40}=134.29°), whereas along the a direction, the ligands forming the square-shaped channels in AEPF-1_{dry} show alternating conformations (for AEPF-1 the torsion angle is C_{12}-C_{11}-C_8-C_5= 146.06°; for AEPF-1_{dry} the alternating torsion angles are C_{29}-C_{28}-C_{25}-C_{24}=49.79° and C_{12}-C_{11}-C_8-C_7=17.11°), as shown in Figure 3C.

These observations suggest that, when a guest molecule enters into a fully open A′ channel (Figure 3C, right), a conformational change occurs, giving the A-type partially open channel (Figure 3C, left) and opening the closed channel A″ (Figure 3C, right), which would be then accessible to other guest molecules. These changes could thus facilitate the migration of each guest molecule to the neighboring unit cell along the channel. Propagation of this process could effectively pump the solvent molecules along the channels throughout the crystal.

Topological study: The networks of both AEPF-1 and AEPF-1_{dry} can be simplified as rods of Ca atoms, running along the b axis, with the organic ligands acting as linkers between Ca nodes from different chains. Connections between them along the [−101] direction are made by two

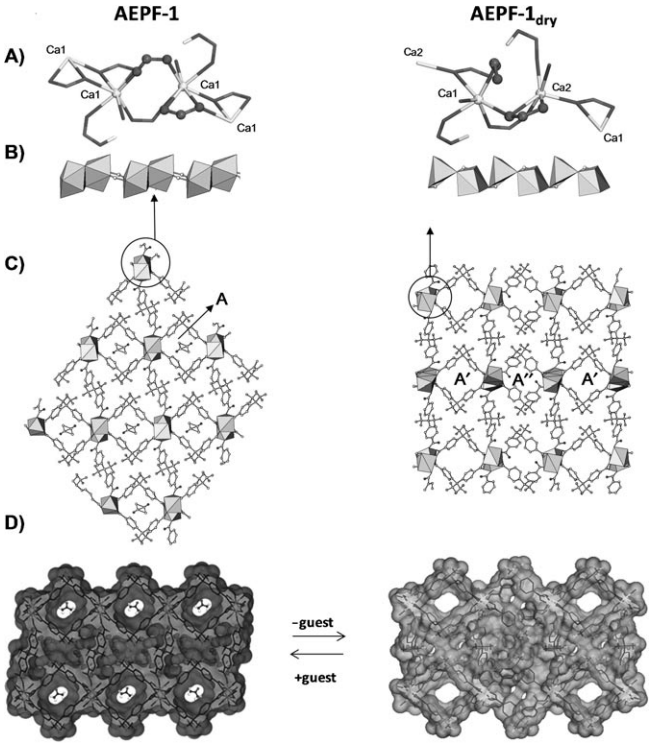

Figure 3. A) Coordination environments for the calcium center of AEPF-1 and AEPF-1_{dry}. B) Polyhedron representation along the *b* direction. C) Structures of both compounds showing the different channels along the *b* direction. D) Connolly surface representation (effectively the inverse of the solvent-accessible surface) for both materials.

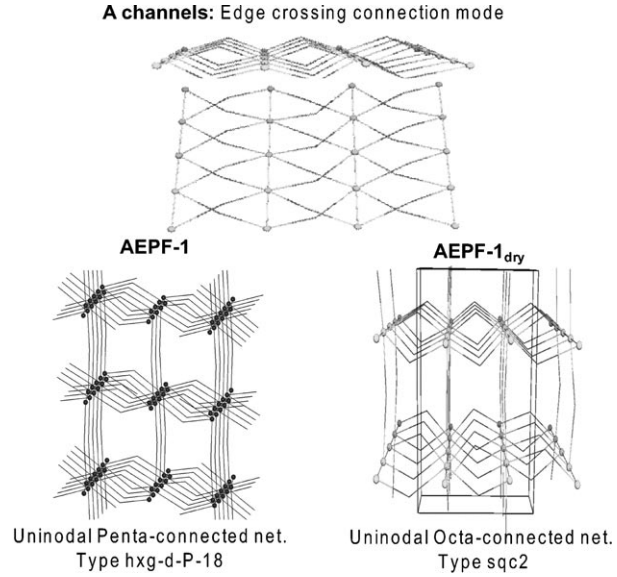

Figure 4. Square-channel and net topology for AEPF-1 and AEPF-1_{dry}.

linkers, above and below the chains, which then gives rise to the typical square channels that appear when using this ligand as a linker.[32–35] These connections exist in both compounds in an edge-crossing manner, similar to those of the LnPF-4 γ-polymorph (A-type channels).[36] However, the ligand can exhibit various torsion angles; when the channels are occupied by the solvent (AEPF-1) all the channels have the same configuration (A type), whereas after extracting the solvent (AEPF-1_{dry}), two kinds of alternated configurations appear (A′ and A″).

The 3D framework for AEPF-1 is a uninodal pentaconnected net, with Schläfli symbol 610 of the type hxg-d-P-18 (vertex symbol [63.63.63.63.63.63.64.65.65.67]) (Figure 4). The AEPF-1_{dry} framework is an uninodal octaconnected net, in which each node is directly joined to two others in the same chain, to four other chains in the *ab* plane, through linkers, and along the *c* direction to two others (Figure 4). The net has a point symbol (425.63) and code sqc2.[37]

Computational studies: In addition to the diffraction experiments, a computational study was also performed to determine the energetic balance between the intrinsic stability of AEPF-1 and the new AEPF-1_{dry} phase. As discussed above, PWDF calculations predicted an accurate 3D structure for AEPF-1_{dry}. Due to the fact that the unit cell volume of AEPF-1_{dry} ($V_{AEPF\text{-}1dry}$) is approximately twice that of AEPF-1 ($V_{AEPF\text{-}1}$), the starting configuration of AEPF-1 was based on a new cell twice as big as the original unit cell. This calculation showed that AEPF-1 is more thermodynamically stable than AEPF-1_{dry}, and allowed us to estimate the energy required for the phase transition ($E_{AEPF\text{-}1}-E_{AEPF\text{-}1dry}$) as 283.9 kJ mol^{-1}.

AEPF-1 phase recovery: The structural analyses described above show that the transformation of AEPF-1 into AEPF-1_{dry} with the loss of acetone guests leads to a new 3D structure. The next step was to investigate the reversibility of this process. Treatment of AEPF-1_{dry} in acetone at room temperature for 2 h (see the Experimental Section), gave the recovered phase named AEPF-1′. This shows that AEPF-1_{dry} can reabsorb acetone guests. To confirm the phase transition, the bulk samples were analyzed by XRPD. As shown in Figure 5, the observed patterns match the simulated ones for AEPF-1 and AEPF-1_{dry}. Note that sample AEPF-1′ shows a pattern closely resembling that of AEPF-1, in accordance with the reversibility of the AEPF-1 to AEPF-1_{dry} phase transition. The differences in relative intensities observed for the Bragg peak centered at 7.2° can be attributed to preferential adsorption of acetone molecules through the plane (101) in AEPF-1′ (Figure 5). Further evidence for readsorption of the guest was obtained by TGA-MS. The TGA curve of AEPF-1′ shows a weight loss of around 5.6 wt% from 75 to 200 °C, which corresponds to the loss of 2.5 acetone molecules per unit cell.

Adsorption by immersion in organic solvents: To investigate whether or not AEPF-1_{dry} can act as an absorber of other organic solvents, experiments were performed by suspending AEPF-1_{dry} samples in a number of different liquids with variable polarity and molecular size/shape (acetone, acetonitrile, 1-butanol, isopropyl alcohol, toluene, benzene, *n*-

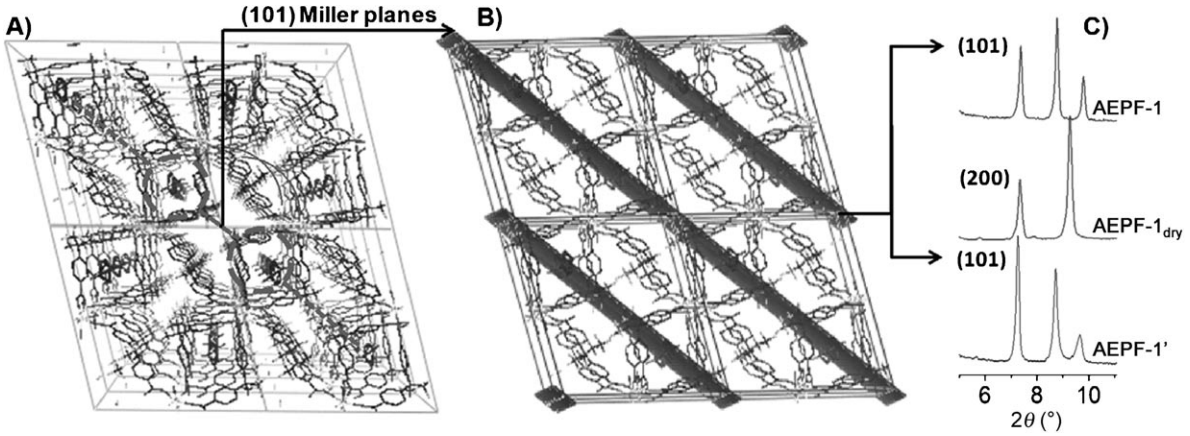

Figure 5. A) AEPF-1 net representation. B) (101) Miller plane representation in AEPF-1. C) Comparison of the X-ray patterns of AEPF-1, AEPF-1_{dry}, and AEPF-1′.

hexane, and isooctane). All these solvents possess a molecular volume that is lower than the pore volume, and should theoretically fit into the cavities of AEPF-1 (Table 1).

Table 1. Sorption properties of AEPF-1_{dry} at 25 °C.

Solvent	Molecular volume[a] [Å^3]	Sorption (molar) [%]	Sorption [wt %]	Solvent molecules per unit cell
toluene	91	16	2.2	1.4[b]
benzene	81	22	2.7	2.3[b]
isopropyl alcohol	64	41	3.8	1.6
1-butanol	79	62	7.1	2.5
acetone	57	70	6.2	2.8
acetonitrile	26	90	5.7	3.6

[a] Approximate volume for each molecule calculated from the van der Waals surface. [b] Number of solvent molecules per unit cell of AEPF-1 according to XRPD data.

AEPF-1_{dry} samples were suspended in each solvent at room temperature for 2 h and then dried in air (see the Experimental Section). TGA-MS was used to evaluate the presence of solvent guest molecules after the treatment (Figure 6A). These studies showed that AEPF-1_{dry} exhibits a huge adsorption capacity in the cases of acetonitrile, acetone, and 1-butanol (ca. 90, ca. 70, and ca. 62 mol % adsorbate, respectively). Note that the linear 1-butanol is strongly adsorbed despite its high molecular volume (see Table 1).

The aromatic solvents (benzene and toluene) were less strongly adsorbed (Figure 6). The nonpolar aliphatic organic solvents (*n*-hexane, isooctane) were not adsorbed at all. These experiments demonstrate the selectivity of AEPF-1_{dry} for small polar organic solvent molecules. The opposite behavior, with selective adsorption of nonpolar organic solvents, was previously reported for a Cu-based MOF.[38]

XRPD was used to check the recovery of the AEPF-1′ phase for AEPF-1_{dry} samples after the treatment. The XRPD patterns corresponding to samples immersed in each solvent are depicted in Figure 6C and D. For polar organic solvents complete recovery of AEPF-1′ is observed (Figure 6C), whereas the sorption behavior for aromatic solvents clearly entails a partial phase conversion (Figure 6D). A profile fitting of XRPD data for each AEPF-1′ sample was performed to determine the structural changes produced in the organic solvent sorption experiments (see the Supporting Information, Section S6).

Selective adsorption by immersion in mixtures of organic solvents: The selective adsorption behavior of AEPF-1_{dry} and AEPF-1′ was examined in four equimolar mixtures of organic solvents: A) acetone/acetonitrile, B) acetone/1-butanol, C) acetone/toluene, and D) acetone/hexane (see the Experimental Section). TGA-MS analyses were performed on AEPF-1_{dry} samples after immersion treatments to evaluate the selectivity of the adsorption process (see Figure 7). For the mixture A, the thermogravimetric profile of AEPF-1′ shows a weight loss of around 6.1 wt % up to 250 °C, which corresponds to the loss of 2.60 acetone molecules and 0.40 acetonitrile molecules per unit cell. For the mixture B, the sample shows a weight loss of around 5.9 wt % up to 250 °C, which corresponds to the loss of 2.10 acetone molecules and 0.50 1-butanol molecules per unit cell. For the mixture C, AEPF-1′ shows a weight loss of around 5.4 wt % up to 275 °C, which corresponds to the loss of 2.48 acetone molecules and 0.05 toluene molecules per unit cell. Finally, for the mixture D, only acetone adsorption is observed, with a weight loss of around 4.9 wt % , which corresponds to the loss of 2.19 acetone molecules per unit cell.

XRPD was used to examine the recovery of all samples of AEPF-1′ (see the Supporting Information, Section S7), which showed that AEPF-1_{dry} not only selectively adsorbs polar organic solvents, but can also selectively separate organic solvents according to their size, shape, or polarity. Such behavior could be important for potential applications of this Ca-based MOF as an adsorbent and/or sensor of organic compounds.

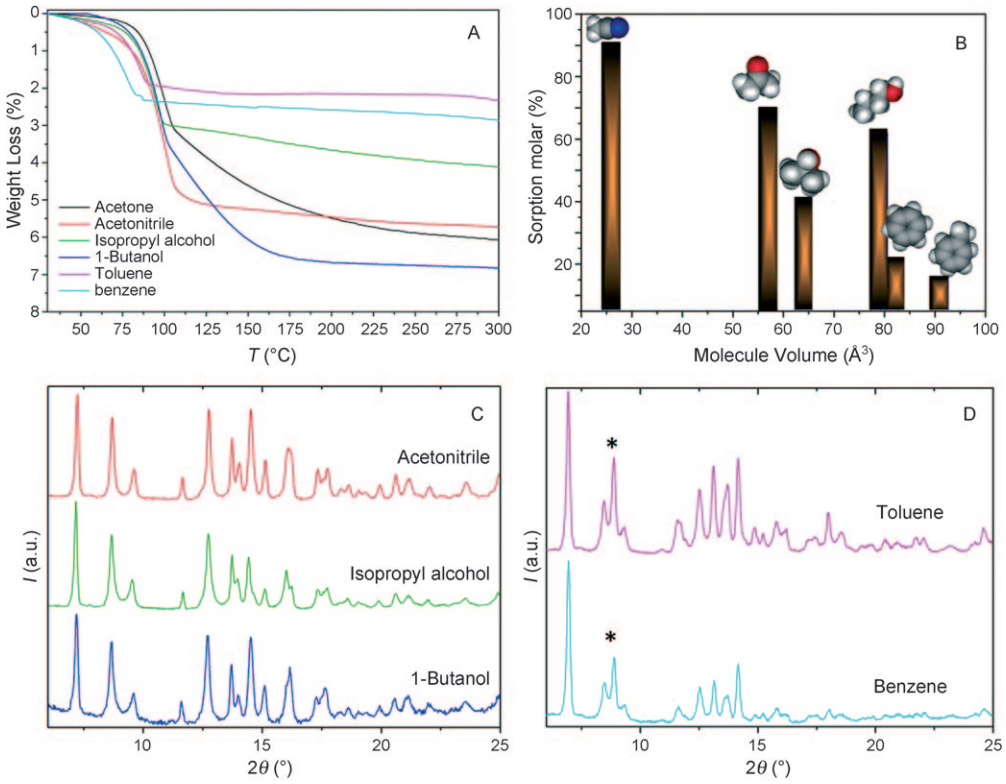

Figure 6. A) TGA under Ar for AEPF-1_{dry} samples after each sorption treatment. B) Plot of molar sorption for each solvent (calculated from TGA-MS) versus molecular volume. C) Comparison of the X-ray patterns for samples after sorption of polar organic solvents. D) Comparison of the X-ray patterns for samples after sorption of aromatic solvents. * denotes the most intense diffraction peak of AEPF-1_{dry}.

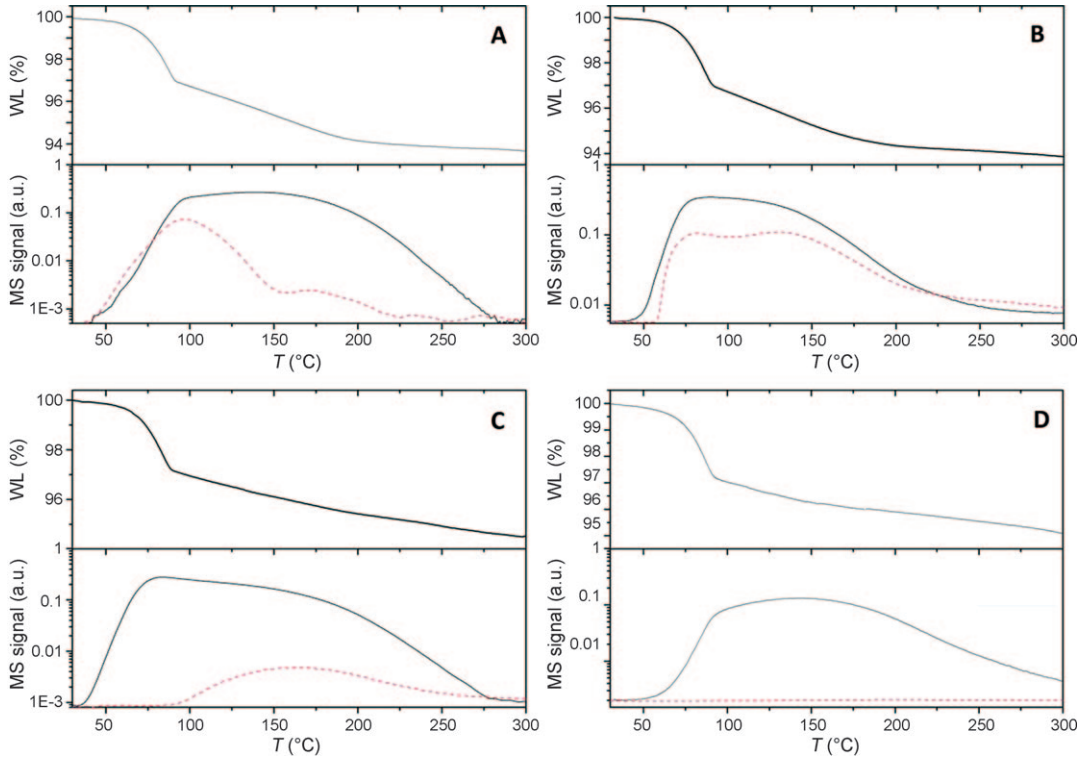

Figure 7. TGA-MS for solvent mixtures: A) acetone (——)/acetonitrile (-----), B) acetone (——)/1-butanol (-----), C) acetone (——)/toluene (-----), and D) acetone (——)/hexane (-----). WL = weight loss.

Conclusion

AEPF-1, a Ca-based MOF, has been synthesized with acetone as a guest molecule. A structural transformation occurs when guest removal takes place (this new phase was named AEPF-1_{dry}) by a crystal to crystal transformation without retention of single-crystal integrity. XRPD and computational studies were applied to determine the structure of the AEPF-1_{dry} phase.

Detailed guest-exchange studies using TGA-MS and XRPD revealed that recoverable guest release/uptake occurs quickly at room temperature, which shows that these structural changes are reversible. Moreover, the special structural properties of this Ca-based MOF lead to the selective adsorption of various organic compounds based on their size, shape, and polarity. This behavior makes AEPF-1 a good candidate for selective solvent adsorption under mild conditions.

Experimental Section

Synthesis: AEPF-1 was synthesized according to published procedures.[21] In brief, a solution of H_2hfipbb (400 mg, 1 mmol) in acetone (9 mL) was added under continuous stirring to a solution of $Ca(CH_3CO_2)_2{\cdot}H_2O$ (178 mg, 1 mmol) in distilled water (10 mL). The resulting mixture was sealed in a Teflon-lined steel autoclave and heated at 170 °C under autogenous pressure for 72 h. The autoclave was then cooled to room temperature, and the product was filtered and washed with distilled water and acetone. The phase purity of the bulk material was independently confirmed by XRPD, TGA, and elemental analysis (see the Supporting Information).

Elemental analysis: Quantitative elemental analyses for AEPF-1 indicated that the C and H ratios were equal to 47.3 and 2.85%, respectively (calcd (%) for AEPF-1: C 48.0, H 2.8). Quantitative elemental analyses for AEPF-1_{dry} indicated that the C and H ratios were equal to 48.27 and 1.97%, respectively (calcd (%) for AEPF-1_{dry}: C 48.67, H 2.39).

Thermogravimetry: TGA was performed by using a Mettler–Toledo apparatus coupled with a mass spectrometer. The experiments were carried out between 25 and 1000 °C in argon (flow rate 50 mL min^{-1}) and at variable heating rates (between 2 and 10 °C min^{-1}). For more information see the Supporting Information.

Infrared spectroscopy: Spectra were recorded in the range 1900–1000 cm^{-1} on a Perkin–Elmer Spectrometer. The spectra of AEPF-1 clearly show the presence of the vibrational bands at around 1650 and 1500 cm^{-1}, characteristic for framework carboxylate groups. A band at 1715 cm^{-1} characteristic for free carbonyl groups is also observed for AEPF-1, which is in agreement with the presence of acetone molecules within the pores of this framework. Variable-temperature experiments were carried out at a heating rate of 2 °C min^{-1}.

Differential scanning calorimetry: DSC was performed at atmospheric pressure by using a Perkin–Elmer DSC-7 calorimeter; 4.7 mg of the sample was placed in a sealed aluminum capsule, and this was heated at 2 °C min^{-1} until melting was observed.

Variable-temperature optical microscopy: A Linkam THMSG-600 stage mounted to a Nikon Eclipse 50iPol Microscope was used to performed VTOM experiments. The sample was placed on a 7 mm quartz coverslip and encased within a pure Ag lid so that it was heated uniformly. The equipment also included a liquid nitrogen cooling system and a TMS94 temperature controller. Images were captured with a Nikon Digital Camera DXM1200F and processed with NIS-Elements Software.

Crystal structure determination: A colorless parallelepiped-shaped crystal of AEPF-1 of dimension $0.14\times0.10\times0.10$ mm^3 was selected under a polarizing optical microscope and mounted on a polyimide micromounts (MiTeGen) with perfluoropolyether oil (Fomblin, Aldrich). Data were collected on a Bruker four circle kappa-diffractometer equipped with a Cu microsource operated at 30 W power (45 kV, 0.60 mA) to generate $Cu_{K\alpha}$ radiation ($\lambda = 1.54178$ Å), with a Bruker AXIOM area detector (microgap technology) at 123 K using an Oxford N-HELIX device (Oxford Cryosystem). Structure resolution details can be found elsewhere.[16] A summary of the main crystallographic data is given in Table S1 (see the Supporting Information).

X-ray powder diffraction: XRPD measurements were performed with a Bruker D8 diffractometer in the θ–θ mode using nickel-filtered $Cu_{K\alpha}$1,2 ($\lambda = 0.15418$ nm) radiation. The best counting statistics were achieved by using a scanning step of 0.02° between 5 and 80° Bragg angles with an exposure time of 0.5 s per step.

Variable-temperature XRPD: Measurements were performed with a Philips X'Pert diffractometer in the θ–θ mode using nickel-filtered $Cu_{K\alpha}$ 1,2 ($\lambda = 0.15418$ nm) radiation. A scanning step of 0.02° was used between 4 and 40° Bragg angles with 1 s per step. To perform in situ XRPD thermodiffraction studies, the diffractometer was equipped with an Anton-Paar chamber. The sample was dispersed on the steel sample holder and heated slowly to 100 °C under vacuum. Each pattern was recorded between 4 and 40° Bragg angles with a scanning step of 0.02° at 1 s per step. The heating rate between temperatures was 2 °C min^{-1}. A final pattern of AEPF-1_{dry} was recorded at 383 K between 4 and 40° Bragg angles with a scanning step of 0.0093° at 1 s per step.

DFT calculations: Periodic DFT calculations were carried out by using a plane wave basis set and the VASP package.[39,40] The initial unit cell parameters and atom positions were taken from the experimental single-crystal and powder X-ray analyses. The data obtained were then fully optimized by using the PW91 implementation of the GGA exchange correlation function[41,42] through the spin-interpolation formula of Vosko–Wilk–Nusair.[43,44] For AEPF-1 and AEPF-1_{dry}, the unit cells contain 251 and 460 atoms, respectively. The effect of the core electrons on the valence electron density was described by the projector augmented wave method[45] implemented by Kresse and Joubert.[46] The valence one-electron Kohn–Sham states have been expanded on a plane wave basis with a cutoff of 415 eV for the kinetic energy. The total energy threshold defining self-consistency of the electron density was set to 10^{-4} eV. The convergence criterion for structural optimization was set to less than 10^{-3} eV, for the difference of total energy from consecutive geometries. Thus, forces on all atoms were ensured to be less than 0.3 eV nm^{-1}. A Gaussian smearing technique with a 0.2 eV width has been applied to enhance convergence. However, all energies presented in the following have been obtained by extrapolating to zero smearing (0 K). Integration in the reciprocal space was carried out by using the Monkhorst–Pack[47] sampling of the Brillouin zone. Several meshes of special k points were used to obtain the desired accuracy in the calculated energies. The apparent energy desorption value was calculated by using a previously published formula.[24] Structural energy transformation was calculated by using the unit cell of AEPF-1_{dry} (twice the unit cell for AEPF-1). In this case both systems have the same number of atoms.

Solvent sorption experiments: Acetone (Cor Química, 99.6%), isopropyl alcohol (Scharlau, 99.5%), acetonitrile (Scharlau, 99.7%), toluene (Riedel de Haen, 99.7%), 1-butanol (Merck, 99%), *n*-hexane (Merck, 99%), isooctane (Scharlau, 99.5%), benzene (Scharlau, 99%), and cyclohexane (Scharlau, 99.7%) were used to determine the selectivity and adsorption capability of AEPF-1_{dry} for various common solvents (polar and nonpolar). A series of post-synthesis treatments of AEPF-1 were performed:

1) Activation. The AEPF-1 was dried (vacuum, 383 K) to remove the extra framework species (acetone molecules) to yield AEPF-1_{dry}. The completeness of conversion of AEPF-1 to AEPF-1_{dry} was tested by means of XRPD data.
2) Solvent sorption experiments. A powder sample of AEPF-1_{dry} was dispersed in various common solvents in a glass holder and vigorously stirred for 4 h at 298 K. The sample was then isolated by centrifugation, and air-dried.

3) Structural and thermogravimetric studies. First, XRPD was performed on the AEPF-1_{dry} sample after sorption experiments (denoted as AEPF-1′) to evaluate structural transformations. Then, TGA-MS was performed to study the desorption process of acetone inside the pores of AEPF-1′.

CCDC-733398 (AEPF-1) and 771413 (AEPF-1_{dry}) contain the supplementary crystallographic data for this paper. These data can be obtained free of charge from The Cambridge Crystallographic Data Centre via www.ccdc.cam.ac.uk/data_request/cif.

Acknowledgements

This work has been supported by the Spanish MCYT Project Mat 2007-60822, CTQ 2007-28909-E/BQU, and Consolider-Ingenio CSD2006-2001. A.E.P.P. acknowledges a JAE fellowship from CSIC and Fondo Social Europeo from EU. V.A.P.O. acknowledges financial support from the MCYT in the Ramón y Cajal research program. A.E.P.P. thanks the group of Prof. Cuevas-Diarte at the University of Barcelona for the valuable help and support in VTOM experiments. The authors thank Dr. Gándara for help with the topological analysis. Computational time has been provided by the Centre de Supercomputació de Catalunya (CESCA).

[1] G. Férey, *Chem. Soc. Rev.* **2008**, *37*, 191.
[2] O. M. Yaghi, M. O'Keeffe, N. W. Ockwig, H. K. Chae, M. Eddaoudi, J. Kim, *Nature* **2003**, *423*, 705.
[3] S. Kitagawa, R. Kitaura, S. I. Noro, *Angew. Chem.* **2004**, *116*, 2388; *Angew. Chem. Int. Ed.* **2004**, *43*, 2334.
[4] X. Lin, X. , J. Jia, P. Hubberstey, M. Schröder, N. R. Champness, *CrystEngComm* **2007**, *9*, 438.
[5] M. B. Duriska, S. M. Neville, J. Lu, S. S. Iremonger, J. F. Boas, C. J. Kepert, S. R. Batten, *Angew. Chem. Int. Ed.* **2009**, *48*, 8919.
[6] M. J. Zaworotko, *Nat. Chem.* **2009**, *1*, 267.
[7] L. Sbircea, N. D. Sharma, W. Clegg, R. W. Harrington, P. N. Horton, M. B. Hursthouse, D. C. Apperley, D. R. Boyd, S. L. James, *Chem. Commun.* **2008**, 5538.
[8] F. Salles, A. Ghoufi, G. Maurin, R. G. Bell, C. Mellot-Draznieks, G. Férey, *Angew. Chem.* **2008**, *120*, 8615; *Angew. Chem. Int. Ed.* **2008**, *47*, 8487.
[9] K. W. Chapman, G. J. Halder, P. J. Chupas, *J. Am. Chem. Soc.* **2009**, *131*, 17546.
[10] S. Kitagawa, K. J. Uemura, *Chem. Soc. Rev.* **2005**, *34*, 109.
[11] R. Kitaura, K. Seki, G. Akiyama, S. Kitagawa, *Angew. Chem.* **2003**, *115*, 444; *Angew. Chem. Int. Ed.* **2003**, *42*, 428.
[12] G. Férey, C. Serre, *Chem. Soc. Rev.* **2009**, *38*, 1380.
[13] P. Horcajada, T. Chalati, C. Serre, B. Gillet, C. Sebrie, T. Baati, J. F. Eubank, D. Heurtaux, P. Clayette, C. Kreuz, J. S. Chang, Y. K. Hwang, V. Marsaud, P. N. Bories, L. Cynober, S. Gil, G. Ferey, P. Couvreur, R. Gref, *Nat. Mater.* **2010**, *9*, 172.
[14] Z. Chun-Feng, Z. Jianyong, W. Qing, C. Zhao-Hua, F. Dieter, S. Cheng-Yong, *Chem. Eur. J.* **2009**, *15*, 7578.
[15] M. C. Das, P. K. Bharadwaj, *J. Am. Chem. Soc.* **2009**, *131*, 10942.
[16] T. Devic, P. Horcajada, C. Serre, F. Salles, G. Maurin, B. Moulin, D. Heurtaux, G. Clet, A. Vimont, J. M. Grenéche, B. L. Ouay, F. Moreau, E. Magnier, Y. Filinchuk, J. M. Marrot, J. C. Lavalley, M. Daturi, G. Férey, *J. Am. Chem. Soc.* **2009**, *131*, 1127.
[17] K. M. Fromm, *Coord. Chem. Rev.* **2008**, *252*, 856–885.
[18] C. Volkringer, T. Loiseau, G. Férey, J. E. Warren, D. S. Wragg, R. E. Morris, *Solid State Sci.* **2007**, *9*, 455.
[19] C. Volkringer, J. Marrot, G. Férey, T. Loiseau, *Cryst. Growth Des.* **2007**, *7*, 685.
[20] C. A. Williams, A. J. Blake, C. Wilson, P. Hubberstey, M. Schröder, *Cryst. Growth Des.* **2008**, *8*, 911.
[21] A. E. Platero-Prats, V. A. de La Peña-O'Shea, M. Iglesias, N. Snejko, Á Monge, E. Gutiérrez-Puebla, *ChemCatChem* **2010**, *2*, 2, 147.
[22] PLATON, A multipurpose Crystallographic Tool, A. L. Spek, Utrecht University, Utrecht, **2005**.
[23] S. Devautour-Vinot, G. Maurin, F. Henn, C. Serre, T. Devic, G. Ferey, *Chem. Commun.* **2009**, 2733.
[24] Apparent energy desorption value was calculated using the formula: $\Delta H_{des} = E_{AEPF\text{-}1} - (E_{AEPF\text{-}1\,(woacetone)} + E_{acetone})$. $E_{AEPF\text{-}1\,(woacetone)}$ = Energy of AEPF-1 without acetone.
[25] D. Louër, M. J. Louer, *J. Appl. Crystallogr.* **1972**, *5*, 271.
[26] A. Boultif, D. Louer, *J. Appl. Crystallogr.* **1991**, *24*, 987.
[27] G. S. Pawley, *J. Appl. Crystallogr.* **1981**, *14*, 357.
[28] Materials Studio Modelling 4.4, http://www.accelerys.com/mstudio/ms_modeling.
[29] V. Favre-Nicolin, R. Cerny, *J. Appl. Crystallogr.* **2002**, *35*, 734.
[30] FOX, Free Objects for Crystallography, http://objcryst.sourceforge.net.
[31] H. M. Rietveld, *J. Appl. Crystallogr.* **1969**, *2*, 65.
[32] L. Pan, M. B. Sander, X. Huang, J. Li, M. Smith, E. Bittner, B. Bockrath, J. K. Johnson, *J. Am. Chem. Soc.* **2004**, *126*, 1308.
[33] A. Monge, N. Snejko, E. Gutierrez-Puebla, M. Medina, C. Cascales, C. Ruiz-Valero, M. Iglesias, B. Gómez-Lor, *Chem. Commun.* **2005**, 1291.
[34] F. Gándara, B. Gómez-Lor, E. Gutiérrez-Puebla, M. Iglesias, M. A. Monge, D. M. Proserpio, N. Snejko, *Chem. Mater.* **2007**, *19*, 72.
[35] F. Gándara, A. de Andrés, B. Gómez-Lor, E. Gutiérrez-Puebla, M. Iglesias, M. A. Monge, D. M. Proserpio, N. Snejko, *Cryst. Growth Des.* **2008**, *8*, 378.
[36] F. Gándara, V. A. de La Peña-O'Shea, F. Illas, N. Snejko, D. M. Proserpio, E. Gutiérrez-Puebla, Á. Monge, *Inorg. Chem.* **2009**, *48*, 4707.
[37] EPINET: Euclidean Patterns in Non-Euclidean Tilings, S. J. Ramsden, V. Robins, S. T. Hyde, S. Hungerford, The Australian National University, 2005–2009, http://epinet.anu.edu.au/.
[38] L. Pan, D. H. Olson, L. R. Ciemnolonski, R. Heddy, J. Li, *Angew. Chem.* **2006**, *118*, 632; *Angew. Chem. Int. Ed.* **2006**, *45*, 616.
[39] G. Kresse, J. Furthmüller, *Comput. Mater. Sci.* **1996**, *6*, 15.
[40] G. Kresse, J. Hafner, *Phys. Rev. B* **1993**, *47*, 558.
[41] J. P. Perdew, Y. Wang, *Phys. Rev. B* **1992**, *45*, 13244.
[42] J. P. Perdew, J. A. Chevary, S. H. Vosko, K. A. Jackson, M. R. Pederson, D. J. Singh, C. Fiolhais, *Phys. Rev. B* **1992**, *46*, 6671.
[43] Y. Zhang, W. Yang, *Phys. Rev. Lett.* **1998**, *80*, 890.
[44] S. H. Vosko, L. Wilk, M. Nusair, *Can. J. Phys.* **1980**, *58*, 1200.
[45] P. E. Blöchl, *Phys. Rev. B* **1994**, *50*, 17953.
[46] G. Kresse, D. Joubert, *Phys. Rev. B.* **1999**, *59*, 1758.
[47] H. J. Monkhorst, J. D. Pack, *Phys. Rev. B* **1976**, *13*, 5188.

Received: May 6, 2010
Published online: August 30, 2010

